DOI 10.24425/aee.2026.158263

Analysis and optimization of permanent magnet linear synchronous motor characteristic with composite magnetic slot wedge

YONGLI LEI[1], CONG GAO[2]✉, YUSHUAI REN[2], GUANG ZHANG[3], YUXI HUANG[2], SHU LI[1], ZHULI LIU[2], SIYUAN JIANG[2], XIAOZHUO XU[2]

[1]*Zhongshan Inspection Branch for Guangdong Institute of Special Equipment Inspection and Research Zhongshan, Guangdong, China*

[2]*School of Electrical Engineering and Automation, Henan Polytechnic University 2001 Shiji Road, Shanyang District, Jiaozuo City, Henan Province, P.R. China*

[3]*The China Electric Power Research Institute Co., Ltd. 15 Xiaoying East Road, Qinghe, Haidian District, Beijing, P.R. China*

e-mail: leiyongli1980A@163.com, ✉ *212507010016@home.hpu.edu.cn,*

(Received: 18.12.2025, revised: 28.04.2026)

Abstract: To suppress cogging force and thrust ripple, a novel composite magnetic slot wedge composed of hard and soft magnetic materials is proposed. A finite element model of a fractional-slot permanent magnet linear synchronous motor is established. First, the effects of non-magnetic, hard magnetic, and soft magnetic slot wedges on electromagnetic characteristics – specifically cogging force and thrust ripple – are compared and analyzed. Subsequently, the composite magnetic slot wedge structure is optimized to determine the ideal material proportion. Finally, the performance of the proposed composite magnetic slot wedge is compared with existing composite slot wedges made of magnetic and non-magnetic materials. The results indicate that the proposed composite magnetic slot wedge provides superior comprehensive optimization of motor performance.

Key words: composite magnetic slot wedge, finite element method, hard magnetic slot wedge, performance analysis, permanent magnet linear synchronous motor

© 2026. The Author(s). This is an open-access article distributed under the terms of the Creative Commons Attribution-NonCommercial-NoDerivatives License (CC BY-NC-ND 4.0, https://creativecommons.org/licenses/by-nc-nd/4.0/), which permits use, distribution, and reproduction in any medium, provided that the Article is properly cited, the use is non-commercial, and no modifications or adaptations are made.

Nomenclature

Abbreviations	Full name
PMLSM	Permanent magnet linear synchronous motor
CMSW	Composite magnetic slot wedge
CSW	Composite slot wedge
NMSW	Non-magnetic slot wedge
HMSW	Hard magnetic slot wedge
SMSW	Soft magnetic slot wedge
FEM	Finite element method
Back-EMF	Back electromotive force
LCM	Least common multiple
THD	Total harmonic distortion

1. Introduction

PMLSMs offer advantages such as high thrust density, fast dynamic response, and simple structure [1–5]; consequently, they are widely employed in systems including cordless vertical lifting, transportation, and logistics [6,7]. However, the slotted structure inevitably induces cogging force and thrust ripple, leading to vibration and acoustic noise. In severe cases, resonance may occur, deteriorating the control performance of the system. Therefore, the suppression of thrust ripple has become a primary focus of current research [8,9].

Currently, strategies to mitigate thrust ripple primarily fall into two categories: control algorithms and structural optimization. On the control side, methods such as repetitive control based on nonlinear feedback [10], deep neural networks [11], and iterative sliding mode control [12] are adopted. In terms of structural design, integral-slot windings feature regular winding arrangement and simple coil insertion processes, boasting advantages such as a straightforward structure, concentrated magnetomotive force fundamental component, and low harmonic content, which have made them viable in traditional motor applications. However, constrained by the laws of pole-slot combination, the interaction between the armature teeth and secondary permanent magnets generates cogging force with a large amplitude. This cogging force is characterized by low harmonic orders and distinct fluctuation periods, directly exacerbating thrust ripple during motor operation and thereby reducing the stability of the motion system. This drawback is particularly prominent in high-precision vertical lifting scenarios and other applications with stringent stability requirements [13,14]. In contrast, fractional-slot windings have shorter end spans, which not only significantly reduce copper usage and copper loss to improve motor energy efficiency but also offer greater flexibility in pole-slot combinations, allowing adjustment of the harmonic characteristics of cogging force through optimized pole-slot ratio design. Although fractional-slot windings have relatively higher spatial harmonic content, rational design of key parameters such as the number of slots per pole per phase and winding connection methods can effectively disperse the energy distribution of cogging force, weaken the dominant role of low-order harmonics, and thus

drastically reduce the peak cogging force and thrust ripple amplitude [15–17]. Considering the core requirements of low ripple and high precision for the long-stroke vertical lifting system studied in this paper, the fractional-slot winding structure is adopted to achieve effective suppression of thrust ripple and improvement of motion control accuracy.

Additionally, techniques such as skewed poles or slots [18], auxiliary teeth [19], and double V-type structures [20] are employed to reduce thrust ripple, but these methods invariably increase manufacturing complexity. To address these challenges, the installation of magnetic slot wedges in the slot openings has been proposed to suppress thrust ripple.

In 1908, the first patent for magnetic slot wedges was granted in Germany, stating that installing magnetic slot wedges in the rotor slots of an electric motor could attenuate the amplitude of magnetic flux passing through the slots during operation, thereby reducing additional losses and motor ripple [21–25].

Mikami *et al*. [21] demonstrated that applying magnetic slot wedges in stator slot openings is an effective means to reduce the harmonic content of the magnetic field. Curiac [22] noted that the use of magnetic slot wedges in large induction motors can improve motor efficiency. Researchers in China began developing and applying magnetic slot wedges in the 1960s. Zhang [23] and Li [24] verified that magnetic slot wedges can, to a certain extent, suppress cogging torque and reduce torque ripple. Huang [25] analyzed the temperature distribution of magnetic slot wedges and concluded that their application significantly reduces the rotor core loss. The aforementioned studies primarily focused on the influence of single-material magnetic slot wedges on the performance of rotating motors and effectively suppressed torque ripple. However, as magnetic slot wedges are exposed to alternating magnetic fields, they are prone to inducing internal eddy currents, resulting in power loss and heat generation. To address this issue, Zhu [26] proposed a composite wedge in 2011 composed of an upper layer of resin glass cloth and a lower layer of magnetic powder; this design weakened the adverse effects of harmonics generated by the variable-frequency power supply on the rotor. In 2012, Tessarolo *et al*. [27, 28] proposed a novel slot wedge design featuring longitudinal hollow slots machined into a standard magnetic wedge and filled with non-magnetic guide rods; this approach reduced cogging torque and enhanced motor robustness. In 2017, Liu *et al*. [29] proposed a double-layer or multi-layer slot wedge composed of alternating magnetic and non-magnetic materials, primarily improving the magnetic properties of railway traction motors. This design was shown to effectively reduce cogging torque and thrust ripple.

This paper focuses on fractional-slot PMLSMs designed for low-vibration and low-loss applications. From a structural design perspective, a novel CMSW is proposed to mitigate thrust ripple and reduce motor losses. First, a finite element model of the fractional-slot PMLSM is established to analyze the structure of the proposed CMSW. The finite element method (FEM) is employed to investigate the influence of non-magnetic materials, hard magnetic materials (ferrite), and soft magnetic materials (silicon steel) on key electromagnetic performance indicators, including the air-gap magnetic field, no-load back electromotive force (back-EMF), cogging force, average thrust, and thrust ripple. Second, by analyzing the electromagnetic properties of the CMSW and the conventional CSW under various composite configurations and dimensional ratios, the optimal structures for both wedge types are determined. Finally, by comparing the thrust ripple and other performance metrics of the two composite wedges against a single-material magnetic slot wedge, the effectiveness of the proposed CMSW in suppressing thrust ripple in fractional-slot PMLSMs is verified.

2. Fractional-slot PMLSM model

As an ideal drive source for direct-drive motion systems, the PMLSM can be categorized into two winding configurations: integer-slot and fractional-slot. When the number of slots per pole per phase, q, is an integer, it is an integer-slot winding; when q is a fraction, it is a fractional-slot winding. The fractional-slot PMLSM typically adopts a concentrated winding structure, which reduces electromagnetic wire usage and copper loss, minimizes motor width, conserves silicon steel, and decreases the volume and mass of the primary core.

However, the fractional-slot configuration increases the harmonic content of the air-gap magnetic flux density, which can lead to intensified vibration and noise. Additionally, the selection of the slot-pole combination significantly affects motor performance, particularly the cogging force. The amplitude of the cogging force is inversely proportional to the least common multiple (LCM) of the number of slots, z, and the number of poles, p. A smaller LCM results in a larger cogging force. Utilizing fewer pole pairs can reduce iron loss, while using fewer slots can simplify manufacturing and improve the slot fill factor. Therefore, to verify the influence of the proposed CMSW on the cogging force, a 3-slot/4-pole ($3s4p$) fractional-slot PMLSM is selected as the object of study. A finite element model is established, with the winding configuration illustrated in Fig. 1. Each tooth carries a concentrated coil, and coils on adjacent teeth are connected in reverse series. Each coil constitutes one phase, resulting in a non-overlapping winding arrangement. The topological structure is presented in Fig. 2. The primary adopts the fractional-slot winding structure, while the secondary consists of alternately arranged N and S permanent magnets. The key structural parameters are listed in Table 1.

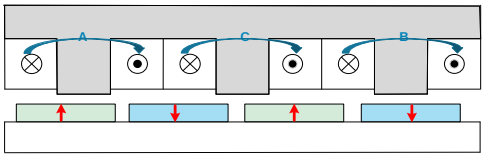

Fig. 1. Plane sketch

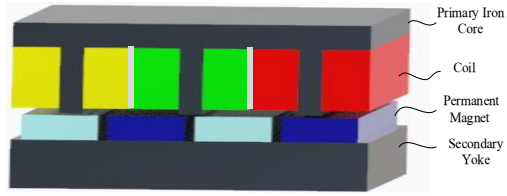

Fig. 2. Topological structure diagram

Table 1. Structural parameters

Parameter name	Value	Unit
Length	180	mm
Pitch distance	45	mm
Depth of groove	30	mm
Tooth width	20	mm
Arc coefficient	0.89	
Number of turns	524	
Rated current	7	A
Permanent magnet materials	NdFeB	

3. Novel composite magnetic slot wedges

3.1. Composite slot wedge

CSWs are defined as wedges composed of two or more distinct materials. Currently, in the field of rotating motors, CSWs consisting of magnetic and non-magnetic materials are widely utilized to enhance motor performance and robustness, demonstrating superior effectiveness compared to single-material magnetic wedges. In contrast, the novel CMSW proposed in this paper is composed of two distinct magnetic materials: hard magnetic and soft magnetic. Based on the material arrangement, the CMSW is classified into two configurations: the upper-lower composite and the left-right composite. The structural diagrams are illustrated in Fig. 3.

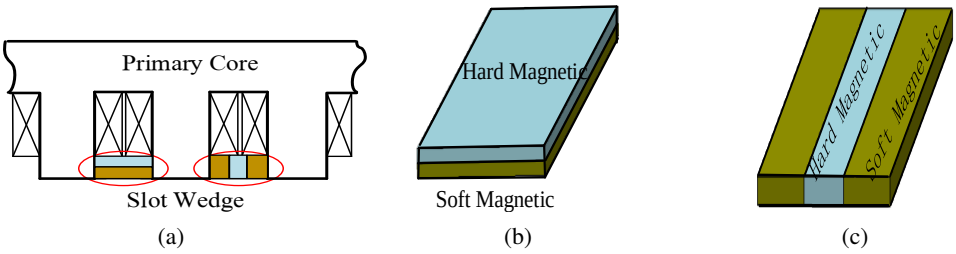

Fig. 3. Structural of CMSW (a); up-down composite structure (b); left-right composite structure (c)

The upper-lower CMSW consists of hard and soft magnetic materials arranged in alternating vertical layers. This configuration can be implemented as either a double-layer or a multi-layer structure. This study specifically focuses on a double-layer structure featuring a hard magnetic upper layer and a soft magnetic lower layer. Conversely, the left-right CMSW comprises hard and soft magnetic materials arranged alternately in the horizontal direction. This design can also be distributed across multiple columns. For the comparative analysis in this paper, a three-column structure consisting of a central hard magnetic section flanked by soft magnetic materials on both sides is adopted.

3.2. Influence of slot wedge materials on electromagnetic characteristics

The design of the CSW is based on the performance optimization principles of single-material slot wedges. Since the electromagnetic performance of the motor varies significantly depending on the wedge material employed, a comparative analysis is essential. To elucidate the influence of different materials and establish a baseline for analyzing the proposed composite wedge, this section investigates the effects of non-magnetic, soft magnetic, and hard magnetic materials on the electromagnetic characteristics of the fractional-slot PMLSM. Key parameters examined include air-gap flux density, no-load back-EMF, cogging force, and steady-state thrust.

1) Air-gap magnetic field distribution

Finite element simulations were conducted for motors equipped with non-magnetic, hard magnetic, and SMSWs, designated as NMSW, HMSW, and SMSW, respectively. To simplify the numerical models and material properties, eddy currents within the iron core were neglected, and the influence of magnetic saturation on the relative permeability of the magnetic wedges was

ignored. Consequently, the relative permeability is assumed to be constant [30]. Figure 4 illustrates the no-load magnetic field and flux density distributions for these three wedge types obtained via two-dimensional finite element analysis.

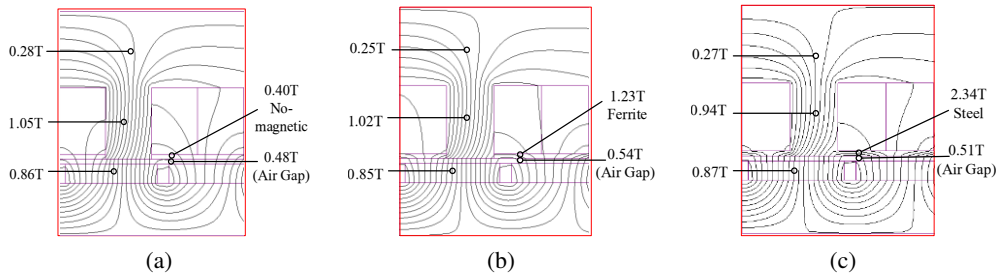

Fig. 4. Distribution of magnetic density: NMSW (a); HMSW (b); SMSW (c)

Based on the no-load air-gap magnetic flux density distribution illustrated in Fig. 4, it is evident that the flux density at the slot openings varies significantly depending on the slot wedge material. With the NMSW, the air-gap flux density near the primary slot openings is lower and unevenly distributed. In contrast, the HMSW and SMSW facilitate the passage of magnetic flux through the wedges, resulting in higher flux densities of 1.23 T and 2.34 T, respectively, and ensuring a smoother flux transition between adjacent teeth. However, during motor operation, variations in the air-gap magnetic flux induce pulsations in the flux density, which directly affect the output force. Furthermore, the harmonic content significantly influences thrust ripple. Figure 5 presents the harmonic content of the air-gap magnetic flux density for the three slot wedge configurations.

As illustrated in the figure, the incorporation of magnetic slot wedges reduces leakage flux, leading to an increase in the amplitude of the air-gap magnetic flux density and its fundamental component. Specifically, with the magnetic slot wedge, the fundamental component reaches 0.81 T, representing a 6% increase compared to the 0.76 T recorded in the absence of the wedge. Furthermore, the HMSW significantly attenuates the 4th, 5th, and 10th harmonics.

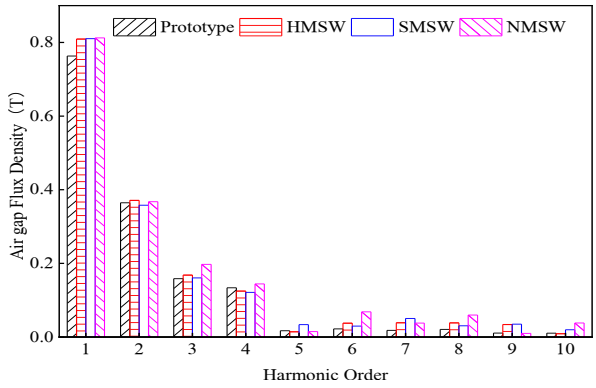

Fig. 5. Air gap magnetic density harmonic analysis

2) Back electromotive force (back EMF)

The distribution of air-gap flux density is closely correlated with the magnitude and total harmonic distortion (THD) of the no-load back-EMF. Specifically, the THD of the no-load back-EMF directly influences the thrust ripple of the motor. The calculation formula for THD is presented in Eq. 1. Achieving an appropriate back-EMF amplitude and a high-quality sinusoidal waveform is critical for ensuring optimal motor performance. The no-load back-EMF waveforms for the NMSW, SMSW, and HMSW configurations were obtained via transient two-dimensional finite element analysis. Furthermore, to compare the harmonic distribution and content, Fourier decomposition was applied to the respective waveforms. Figure 6 displays the no-load back-EMF waveforms and their corresponding harmonic spectra.

$$\mathrm{THD} = \frac{\sqrt{E_2^2 + E_3^2 + \ldots + E_{10}^2}}{E_1}. \tag{1}$$

As illustrated in Fig. 6, under the same operating conditions, the no-load back EMF peak values of the four structures (slotless wedge, HMSW, SMSW, and NMSW) are 304 V, 307 V, 281 V, and 303 V respectively. It can be observed that the addition of HMSW leads to a slight increase in the peak value of the no-load back EMF.

Their corresponding fundamental component amplitudes are 312 V, 308 V, 284 V, and 312 V, respectively. It is evident that compared with the structure of slotless wedge, the other three structures with slot wedges (HMSW, SMSW, and NMSW) all result in a reduction in the fundamental component amplitude of the motor's back EMF.

The THD values, calculated using Eq. 1 for the four cases, are 2.3%, 1.2%, 2.2%, and 2.3%, respectively. Consequently, the HMSW yields the lowest waveform distortion rate, demonstrating its superior capability in optimizing the back-EMF waveform and suppressing harmonics.

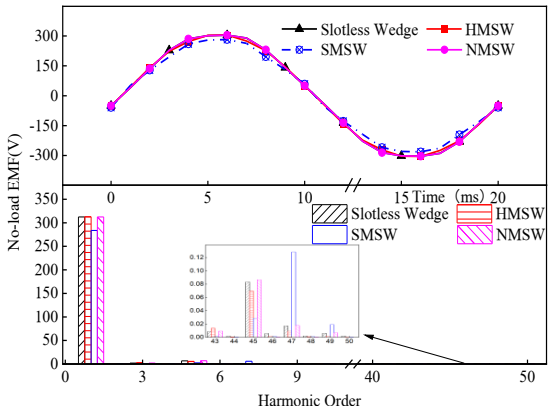

Fig. 6. No-load back EMF and harmonic analysis

3) Cogging force

Cogging force is a primary source of thrust ripple in electrical machines. It arises principally from the slotted structure of the motor core, which induces periodic variations in the air-gap magnetic flux density. To isolate the cogging force by eliminating the influence of end effects,

periodic boundary conditions are applied to the lateral boundaries of the model, while a Dirichlet boundary condition, specifically $A_Z = 0$, is imposed on the upper and lower boundaries. The resulting cogging force waveform is presented in Fig. 7.

As illustrated in Fig. 7, the cogging force exhibits a periodic variation with a period defined as 1/(*s***p*), where 1 denotes the total length of the motor. Notably, the waveforms for the NMSW and the slotless wedge cases are effectively superimposed. The peak-to-peak cogging force for the SMSW differs from the slotless case by only 2 N. In contrast, the HMSW significantly reduces the peak-to-peak value to 9 N, representing an 86.6% reduction. This demonstrates that the HMSW possesses a substantial capability to suppress cogging force.

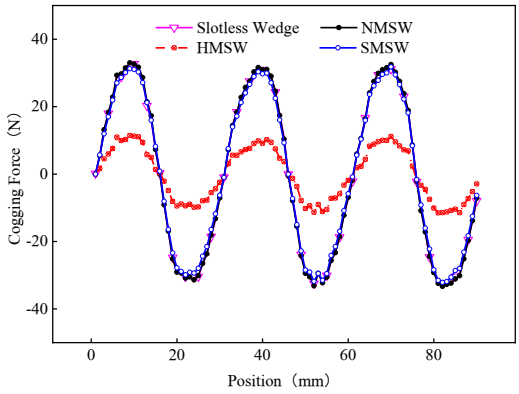

Fig. 7. Cogging force curve

4) Steady-state thrust

The electromagnetic thrust of a PMLSM results from the interaction between the magnetic field produced by the primary winding and the permanent magnets on the secondary side [19]. This parameter serves as a critical metric for evaluating motor performance. Figure 8 and Fig. 9 illustrate the steady-state thrust waveforms and permanent magnet losses, respectively, obtained via finite element analysis for various slot wedge materials. Detailed quantitative data are summarized in Table 2. Thrust ripple is defined as the ratio of the difference between the maximum and minimum thrust to the average thrust, as expressed in Eq. 2.

$$K_r = \frac{F_{\max} - F_{\min}}{F_{\text{avg}}}, \tag{2}$$

where $F_{\max}$ represents the maximum thrust, $F_{\min}$ represents the minimum thrust, and F_{avg} denotes the average thrust.

The results indicate that the NMSW exerts negligible influence on the average thrust and ripple of the motor. In contrast, the SMSW and HMSW reduce the average thrust by 122 N and 16 N, respectively, while increasing the normal force. Notably, the HMSW significantly suppresses fluctuations in both the thrust and the normal force. Consequently, the HMSW demonstrates superior overall performance, characterized by a mere 1.6% reduction in average thrust and a 72% reduction in normal force ripple, while also yielding the lowest permanent magnet loss.

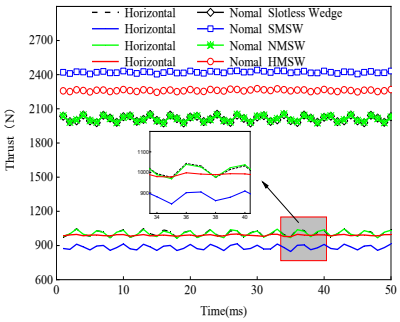

Fig. 8. Electromagnetic thrust

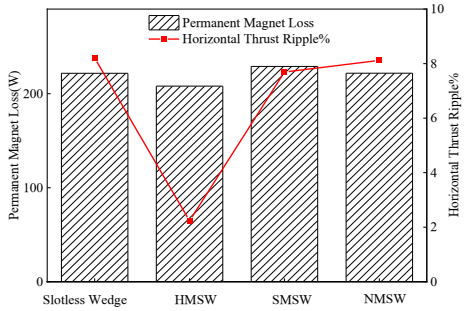

Fig. 9. Permanent magnet loss and horizontal trust ripple

Table 2. Thrust and ripple magnitude

	Horizontal/normal thrust (N)	**Horizontal/normal ripple (%)**
Slotless wedge	1 006/2 012	8.2/3.8
NMSW	1 005/2 013	8.1/3.9
SMSW	884/2 401	7.7/4.1
HMSW	990/2 261	2.3/1.4

4. Optimization of composite magnetic slot wedges

As illustrated in Fig. 10, This section analyzes the data relative to the proportion coefficient $k_1(k_1 = H_1/H = L_1/L)$ for the two composite configurations to determine the optimal dimensional parameters for the wedges. Subsequently, the electromagnetic characteristics of the motor – specifically average thrust, thrust ripple, cogging force, and permanent magnet loss – are compared using the optimized dimensions of both the CSW and the CMSW.

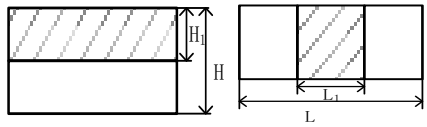

Fig. 10. CMSW section diagram

4.1. Optimization of hard magnetic and non-magnetic composite wedges

The analysis in Section 2 indicates that the NMSW exerts negligible influence on motor performance, whereas the HMSW significantly suppresses thrust ripple. In the field of rotating electrical machines, CSWs, are widely employed instead of single-material magnetic wedges to mitigate cogging torque, enhance mechanical robustness, and reduce the eddy current losses generated within the wedge itself. Figure 11 and Fig. 12 illustrate the average thrust, thrust ripple, permanent magnet loss, and cogging force as functions of the proportion coefficient k_1.

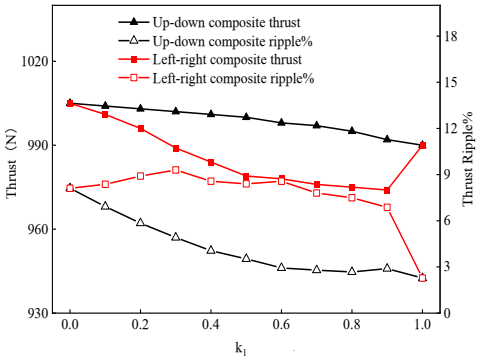

Fig. 11. Contrast of thrust and ripple

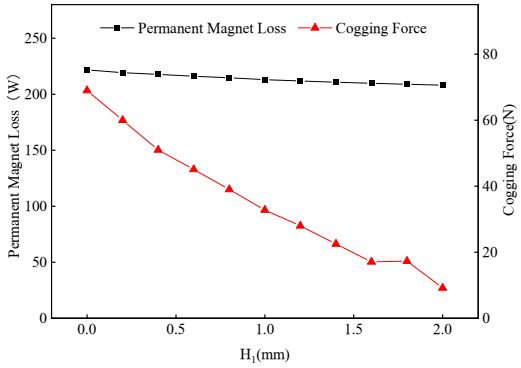

Fig. 12. Permanent magnet loss and cogging force

As illustrated in Fig. 11, the average thrust for both composite configurations decreases as k_1 increases. However, the thrust of the vertically composite wedge consistently exceeds that of the horizontally composite wedge, while its thrust ripple remains lower. Consequently, it is concluded that the vertically composite structure offers superior performance for the fractional-slot PMLSM. Figure 12 depicts the permanent magnet loss and cogging force for the vertically composite wedge as a function of the ferrite height H_1. The results indicate that optimal performance is achieved when the ferrite height H_1 is 1.6 mm. At this dimension, the thrust ripple and cogging force are minimized, and the permanent magnet loss is reduced. Specifically, compared with the single-material ferrite wedge, the composite design results in a 5 N decrease in average thrust, a 25.6% reduction in thrust ripple, an 8N increase in cogging force, and a 2 W reduction in permanent magnet loss. This configuration achieves an optimal balance, combining the high thrust characteristic of non-magnetic wedges with the low ripple capability of hard magnetic wedges.

4.2. Optimization of hard magnetic and soft magnetic composite wedges

Both hard magnetic ferrite and soft magnetic silicon steel possess high resistivity and magnetic permeability, properties that contribute to the reduction of eddy current losses. However, ferrite is characterized by lower magnetic energy storage per unit volume, whereas silicon steel exhibits greater eddy current losses at elevated operating frequencies. Consequently, combining these materials can achieve both low-frequency compensation and high-frequency filtering. The average thrust and thrust ripple are analyzed as functions of the proportion coefficient k_1, with the results illustrated in Fig. 13.

As illustrated in Fig. 13, as the proportion coefficient k_1 increases, the average motor thrust exhibits an upward trend, whereas the thrust ripple shows a downward trend. When $k_1 < 0.2$, both the average thrust and the ripple of the vertically composite wedge exceed those of the horizontally composite wedge. Conversely, when $k_1 > 0.2$, the thrust and ripple of the horizontally composite wedge surpass those of the vertically composite wedge. The thrust ripple reaches its minimum when $H_1 = 1.8$ mm, representing an 82% reduction compared to the slotless case.

Figure 14 depicts the permanent magnet loss and cogging force as functions of k_1. It is evident that the loss associated with the vertically composite wedge decreases continuously and remains lower than that of the horizontally composite wedge.

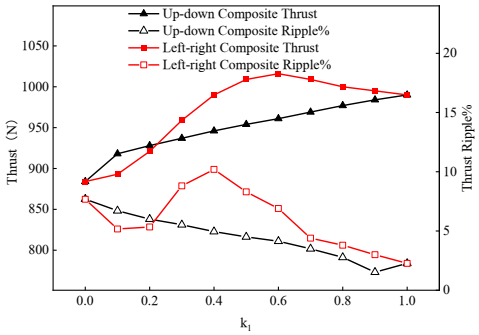

Fig. 13. Comparison of thrust and ripple

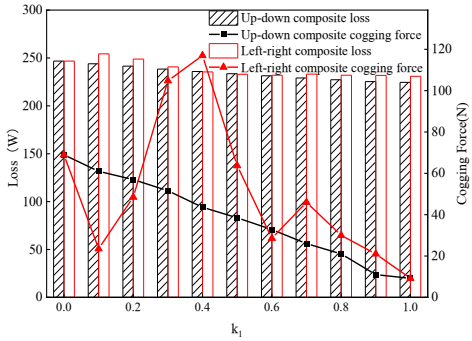

Fig. 14. Loss and cogging force

Furthermore, the cogging force of the vertically composite wedge demonstrates a linear decrease, whereas the cogging force of the horizontally composite wedge exhibits irregular behavior with larger magnitudes. In conclusion, optimal motor performance is achieved using the vertically CMSW with $H_1 = 1.8$ mm. Compared to the single-material ferrite wedge, the average thrust is reduced by 6 N, but the thrust ripple is decreased by 32.9%, indicating that the overall optimization effect is superior to that of the conventional CSW.

5. Summary

Based on the finite element analysis, the optimal configurations and dimensional ratios for the two CSW designs were determined. To further demonstrate the superiority of the CSW over the single-material magnetic slot wedge, and to verify that the composite wedge utilizing two magnetic materials outperforms the combination of magnetic and non-magnetic materials, the cogging force, detent force, and thrust of the optimized composite wedges are compared with those of the single-material magnetic wedge in Fig. 15, Fig. 16, and Fig. 17. Detailed performance metrics are summarized in Table 3.

As illustrated in the figures, all three wedge configurations significantly suppress cogging force, detent force, and thrust ripple. The detent force magnitudes for the three cases correspond to only 3.4%, 4.2%, and 4.1% of the average thrust, respectively. It is observed that the HMSW exhibits the most pronounced effect in suppressing detent force. However, the CMSW demonstrates superior capability in reducing both thrust ripple and normal force ripple, while simultaneously yielding the lowest permanent magnet loss.

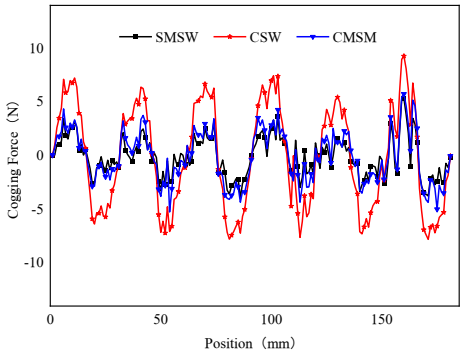

Fig. 15. Cogging force

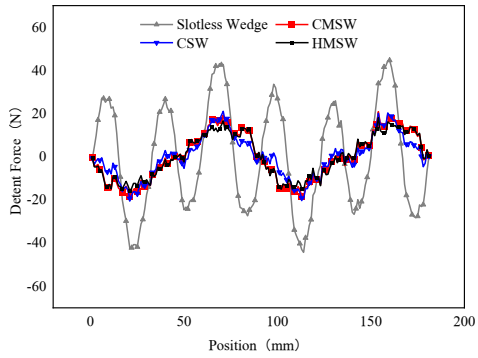

Fig. 16. Detent force

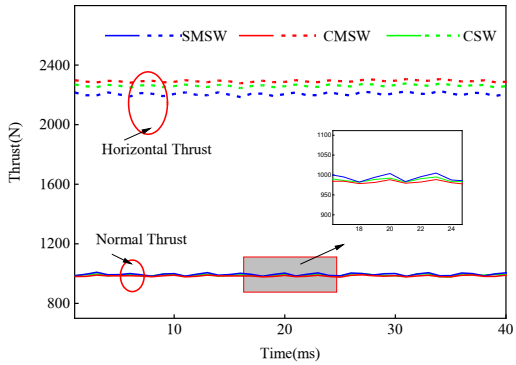

Fig. 17. Distribution of the steady force

Table 3. Performance date of each slot wedge

	Horizontal/ normal thrust (N)	**Horizontal/ normal ripple (%)**	**Peak-to-peak cogging force (N)**	**Peak-to-peak detent force (N)**	**Loss (W)**	**Efficiency (%)**
Slotless wedge	1 006/2 012	8.2/3.8	67	89	237	93.2
HMSM	990/2 261	2.3/1.4	9	34	231	93.1
CSW	985/2 270	1.7/1.5	17	41	229	93.1
CMSW	984/2 292	1.5/1.2	11	40	229	93.1

6. Conclusion

To address the stringent low-ripple requirements of cordless vertical lifting systems, this paper proposes a novel CMSW, comprising two distinct magnetic materials. Using a 3-slot/4-pole PMLSM as the research object, a finite element model was established to analyze the

influence of non-magnetic, soft magnetic, and hard magnetic materials on key performance metrics, including air-gap magnetic field distribution, no-load back-EMF, and steady-state thrust. The initial analysis indicated that the HMSW offered superior optimization effects compared to other single-material configurations. Subsequently, the optimal wedge structure was determined by evaluating the electromagnetic performance of the PMLSM under various composite configurations and dimensional ratios. Finally, a comparative analysis between the optimized CMSW and the single-material HMSW verified1 that the proposed composite wedge effectively suppresses thrust ripple. The specific conclusions are summarized as follows:

1. Under identical conditions, the HMSW provides superior performance optimization compared to both soft magnetic and NMSW. The optimization effect is maximized when the relative permeability is 3. Compared to the slotless case, the average thrust decreases by 16 N, but the thrust ripple is reduced by 72%; the normal force increases by 259 N, while its ripple decreases by 63.2%. Additionally, the cogging force is reduced by 86.6% and losses are lowered by 6W, demonstrating significant improvements in ripple suppression and loss reduction.
2. Under the same conditions, the CSW composed of hard and non-magnetic materials achieves optimal performance when configured with a vertically composite structure and a ferrite height of $H_1 = 1.6$ mm. Specifically, the average thrust is reduced by 21 N, while the thrust ripple is decreased by 79%, the normal force ripple by 60.5%, the cogging force by 74.6%, and the losses by 8W.
3. Similarly, the CMSW composed of hard and soft magnetic materials demonstrates optimal performance when configured with a vertically composite structure and a ferrite height of $H_1 = 1.8$ mm. This configuration results in a 22 N reduction in average thrust while achieving substantial ripple suppression: thrust ripple decreases by 82%, normal force ripple by 68.4%, and cogging force by 83.6%. Additionally, the power loss is reduced by 8 W.
4. Among the single-material magnetic slot wedge, CSW, and CMSW, although the thrust of the CMSW is reduced by 2%, it exhibits the smallest thrust ripple, lower loss, and does not reduce motor efficiency.

Acknowledgements

This work was supported in part by the Natural Science Foundation of Henan Province (252300423398, 252300423322), Key Technologies R&D Program of Henan Province of China (NO. 252102241054), Doctoral Foundation of Henan Polytechnic University (B2024-23, B2025-35), The Fundamental Research Funds for the Universities of Henan Province (NSFRF2502039).

References

[1] Juncai Song, Fei Dong, Jiwen Zhao, *Design optimization research of air-core permanent magnet synchronous linear motor based on gravity neighborhood center algorithm*, Proceedings of the CSEE, vol. 37, no. 12, pp. 3594–3601+3688 (2017).

[2] Yuetong Xu, Jianzhong Fu, *Thrust ripple optimization and experiment for PMLSM*, Proceedings of the CSEE, vol. 25, no. 12, pp. 122–126 (2005).

[3] Li Z., Yue S., Guo P., Zhou J., Li Y., *Efficient and Accurate Electromagnetic-Analysis Model for Asymmetric-End Permanent Magnet Linear Synchronous Motor*, IEEE Transactions on Energy Conversion (2025), DOI: 10.1109/TEC.2025.3648999.

[4] Yin L., Zhao J., Pan Z., Yu Z., Xu R., *Fault Detection of Microcracks in Permanent Magnet of Permanent Magnet Synchronous Linear Motors Based on Magnetic Surface Information Time-Domain and Gray Texture Features*, IEEE Transactions on Transportation Electrification, vol. 12, no. 1, pp. 986–997 (2026), DOI: 10.1109/TTE.2025.3624564.

[5] Wu T., Xue G., Lei G., Guo Y., Zhu J., *A Hybrid Electromagnetic Model of Tubular Permanent Magnet Linear Synchronous Motors Based on Transfer Learning*, IEEE Transactions on Industrial Electronics, vol. 73, no. 2, pp. 2758–2767 (2026), DOI: 10.1109/TIE.2025.3594456.

[6] Jianglong Yan, Yanzhe Li, Yimeng Yang, Guoqing Liu, Yuantao Liu, *Cooperative optimization of temperature and thrust ripple in permanent magnet synchronous linear motors*, Archives of Electrical Engineering vol. 74, no. 2, pp. 503–519 (2025), DOI: 10.24425/aee.2025.153911.

[7] Zhang M., Guo L., Lu W., *Optimization of Permanent Magnet Linear Motors Based on Improved Finite Difference Method*, IEEE, vol. 14, pp. 13413–13422 (2026), DOI: 10.1109/ACCESS.2026.3656865.

[8] Liu X., Zhao Z., Ji Y., Huang L., Jia W., Qiu H., *Design and Optimization of High-Precision Permanent Magnet Synchronous Linear Motor with Composite Mover*, IEEE Transactions on Magnetics (2026), DOI: 10.1109/TMAG.2026.3662095.

[9] Liu X., Zhao Z., Jia W., Ji Y., Fu D., Qiu H., *Electromagnetic Vibration Reduction of a Magnetic Induction Modulated Permanent Magnet Synchronous Linear Motor*, IEEE Transactions on Transportation Electrification, vol. 12, no. 1, pp. 566–577 (2026), DOI: 10.1109/TTE.2025.3618873.

[10] Gaojun Meng, Haitao Yu, Minqiang Hu, *Thrust Ripple Suppression for Linear Flux-Switching Permanent Magnet Machine Based on a Repetitive Control Strategy of Nonlinear Feedback*, Transactions of China Electrotechnical Society, vol. 32, no. 8, pp. 169–177 (2017), DOI: 10.19595/j.cnki.1000-6753.tces.2017.08.020.

[11] Yang Yang, Jiwen Zhao, Juncai Song, *Structural Optimization of Air-core Permanent Magnet Synchronous Linear Motors Based on Deep Neural Network Models*, Proceedings of the CSEE, vol. 39, no. 20, pp. 6085–6094+6189 (2019).

[12] Leyang Yan, Peiqing Ye, Hui Zhang *et al.*, *Disturbance rejection for linear motor based on multi-periodic learning variable structure control*, Electric Machines and Control, vol. 21, no. 1, pp. 8–13 (2017).

[13] Liu Jiwei, Di Chong, Li Shihao, Bao Xiaohua, *Analysis and Mitigation of Torque Ripple of a Dual-Stator Low-Speed High-Torque Permanent Magnet Machine with Different Winding Forms*, Transactions of China Electrotechnical Society, vol. 39, no. 12, pp. 3646–3657 (2024).

[14] Bao Xiaohua, Zhu Ran, Liu Jiwei, Li Shihao, *Torque Ripple Analysis of Dual-Stator Surface Mounted Low-Speed High-Torque Permanent Magnet Synchronous Motors Based on Phase Analysis*, Transactions of China Electrotechnical Society, vol. 37, no. 22, pp. 5660–5669 (2022).

[15] Xiang Zhao, Yu Fan, Jing Xia *et al.*, *Rotor structure to reduce rotor losses of permanent magnet electric machines*, Electric Machines and Control, vol. 23, no. 2, pp. 62–67 (2019).

[16] Baoquan Kou, Qingwen Ge, Haoquan Zhang, Xu Niu, Changchuang Huang, *Design and Analysis of Double-Sided Dislocated High Speed Permanent Magnet Linear Synchronous Motors*, Transactions of China Electrotechnical Society, vol. 36, no. 6, pp. 1149–1158 (2021).

[17] Liu Zhiguang, Yang Zhiyong, Wang Xiaoyuan, Yu Pengcheng, Li Zhiqiang, *Design of multi-phase permanent magnet synchronous motor with fractional-slot windings for electromagnetic vibration reduction considering stator teeth modulation*, IET Electric Power Applications, vol. 17, no. 9, pp. 1123–1135 (2023), DOI: 10.1049/elp2.12327.

[18] Songning Shi, Dazhi Wang, *Influences of magnet skewing parameters on cogging torque and optimization of permanent magnet drive*, Electric Machines and Control, vol. 19, no. 9, pp. 337–343 (2015).

[19] Baoquan Kou, He Zhang, Shoulun Guo *et al*., *End Effect Detent Force Reduction for Permanent Magnet Linear Synchronous Motors with Auxiliary Poles One-Piece Structure*, Transactions of China Electrotechnical Society, vol. 30, no. 6, pp. 106–113 (2015).

[20] Bing Peng, Liping Li, Nan Zhang *et al*., *A method for reducing force fluctuation by double-V-shaped structure in permanent magnet linear motor*, Transactions of China Electrotechnical Society, vol. 32, no. 22, pp. 108–114 (2017).

[21] Mikami H., Ide K., Arai K., Takahashi M., Kajiwara K., *Dynamic harmonic field analysis of a cage type induction motor when magnetic slot wedges are applied*, IEEE Transactions on Energy Conversion, vol. 12, no. 4, pp. 337–343 (1997), DOI: 10.1109/60.638870.

[22] Curiac R., Li H., *Improvements in energy efficiency of induction motors by the use of magnetic wedges*, 2011 Record of Conference Papers Industry Applications Society 58th Annual IEEE Petroleum and Chemical Industry Conference (PCIC), Toronto, ON, Canada, pp. 1–6 (2011), DOI: 10.1109/PCICon.2011.6085890.

[23] Haijun Zhang, Jingjun Zhang, Ruizhen Gao, *Using magnetic slot wedge to improve the air-magnetic field of brushless direct current motor*, Journal of North China Electric Power University, vol. 34, no. 3, pp. 17–21+40 (2007).

[24] Jun Li, Ying Liu, Zigui Xu *et al*., *Properties of Laminated Magnetic Wedge and Their Effects on Characteristics of Motors*, Proceedings of the CSEE, vol. 25, no. 16, pp. 126–131 (2005).

[25] Dongzhu Huan, Weili Li, Yaoyu Wang, *Influence of magnetic slot wedge on rotor losses and temperature field of PMSM*, Electric Machines and Control, vol. 20, no. 1, pp. 60–66 (2016).

[26] Shouqing Zhu, Qiang Yang, Zhiqiang Liu, *Composite Wedge of Rotor for Frequency Conversion Motor*, CN202334060U (2012).

[27] Tessarolo A., Luise F., Bortolozzi M., Mezzarobba M., *A new magnetic wedge design for enhancing the performance of open-slot electric machines*, 2012 Electrical Systems for Aircraft, Railway and Ship Propulsion, Bologna, Italy, pp. 1–5 (2012), DOI: 10.1109/ESARS.2012.6387432.

[28] Tessarolo A., Luise F., Mezzarobba M., Bortolozzi M., Branz L., *Special magnetic wedge design optimization with genetic algorithms for cogging torque reduction in permanent-magnet synchronous machines*, 2012 Electrical Systems for Aircraft, Railway and Ship Propulsion, Bologna, Italy, pp. 1–6 (2012), DOI: 10.1109/ESARS.2012.6387431.

[29] Huaicong Liu, Sooyoung Cho, Hyun-Seok Hong *et al*., *Comparative Analysis of Magnetic Slot Wedges Design for Increasing Performance of Railway Traction Motor*, Journal of Electrical Engineering and Technology, vol. 12, no. 6, pp. 2411–2418 (2017), DOI: 10.5370/JEET.2017.12.6.2411.

[30] Ming Cheng, Zhou E., *Analysis, calculation of pull-in performance of the permanent magnet synchronous motors*, Proceedings of the CSEE, vol. 16, no. 2, pp. 130–134 (1996).